Electronic Supplementary Material (ESI) for Energy & Environmental Science.
This journal is © The Royal Society of Chemistry 2020

SUPPLEMENTARY INFORMATION

Lithium Degradation in Lithium-Sulfur Batteries: Insights into Inventory Depletion and Interphasial Evolution with Cycling

Sanjay Nanda and Arumugam Manthiram*

Materials Science and Engineering Program and Texas Materials Institute, The University of Texas at Austin, Austin, TX78712, USA

*Corresponding author: Tel: +1-512-471-1791; fax: +1-512-471-7681.
E-mail address: manth@austin.utexas.edu (A. Manthiram)

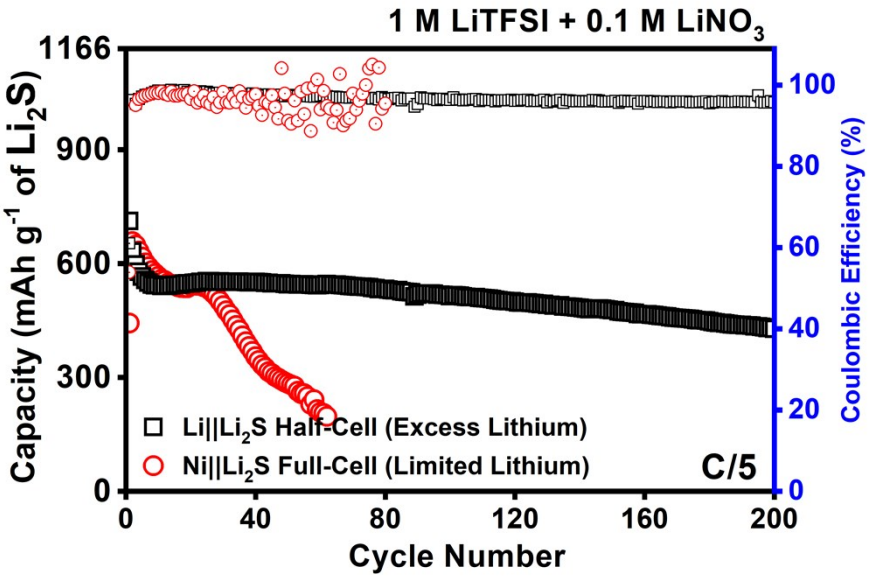

Fig. S1. Electrochemical performance of the Li || Li_2S half cell and anode-free Ni || Li_2S full cell at C/5 (1 mA cm^{-2}) rate, shown here for an extended cycling period of 200 cycles. The increase in applied current leads to poor efficiencies of lithium plating stripping, which brings about faster capacity fade at C/5 rate compared to C/10 rate. The lithium inventory loss rate (LILR) increases from 0.6% per cycle at C/10 rate to 1.8% per cycle at C/5 rate. Meanwhile, the half cell shows minor changes in electrochemical performance from C/10 rate to C/5 rate, with the sulfur inventory loss rate only increasing from 0.2% per cycle to 0.3% per cycle. Thus, the constraints on electrochemical performance imposed by a limited lithium inventory become more apparent at a higher current rate.

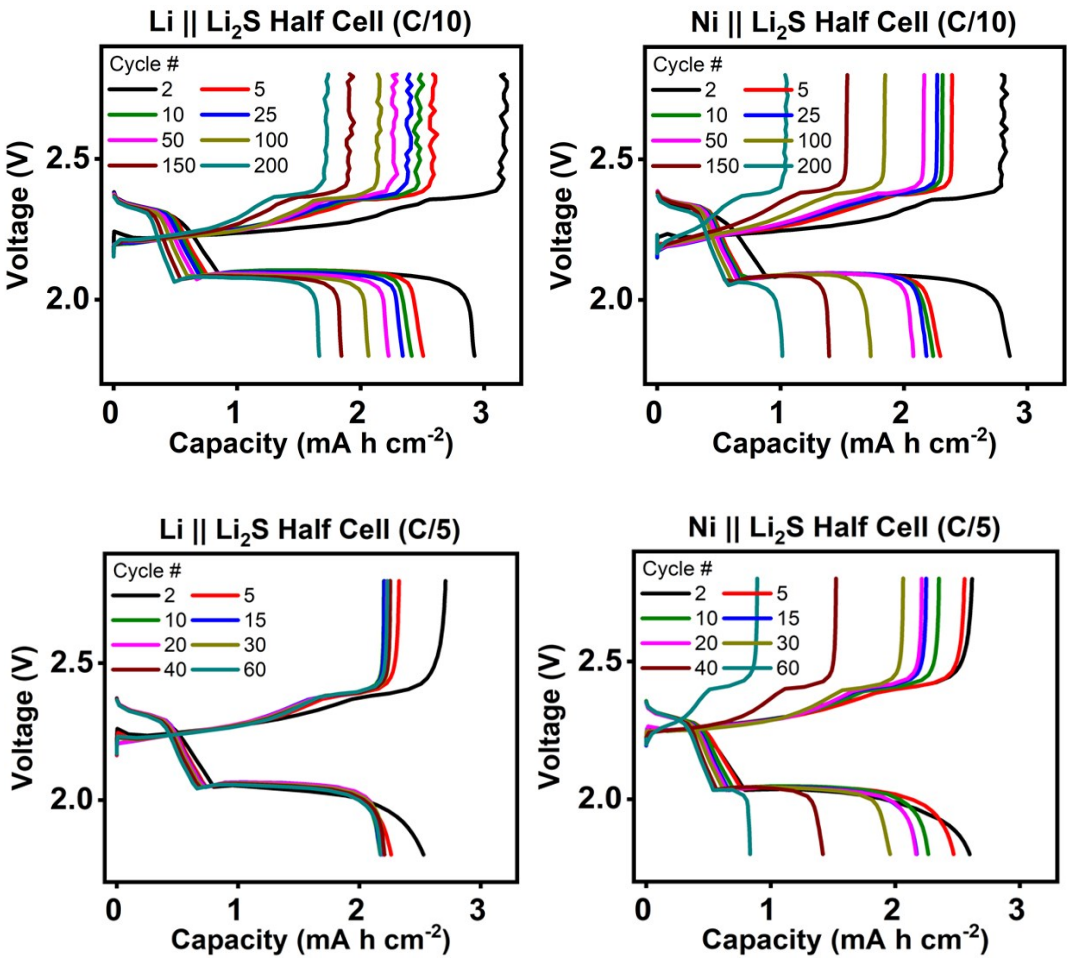

Fig. S2. Charge/discharge curves showing the increase in polarization for the Li || Li_2S half cell and anode-free Ni || Li_2S full cell at C/10 rate. Different cycle numbers from 2 to 200 cycles are covered. Charge/discharge curves are also shown to demonstrate the increase in polarization for the Li || Li_2S half cell and anode-free Ni || Li_2S full cell at C/5 rate. Different cycle numbers from 2 to 60 cycles are covered.

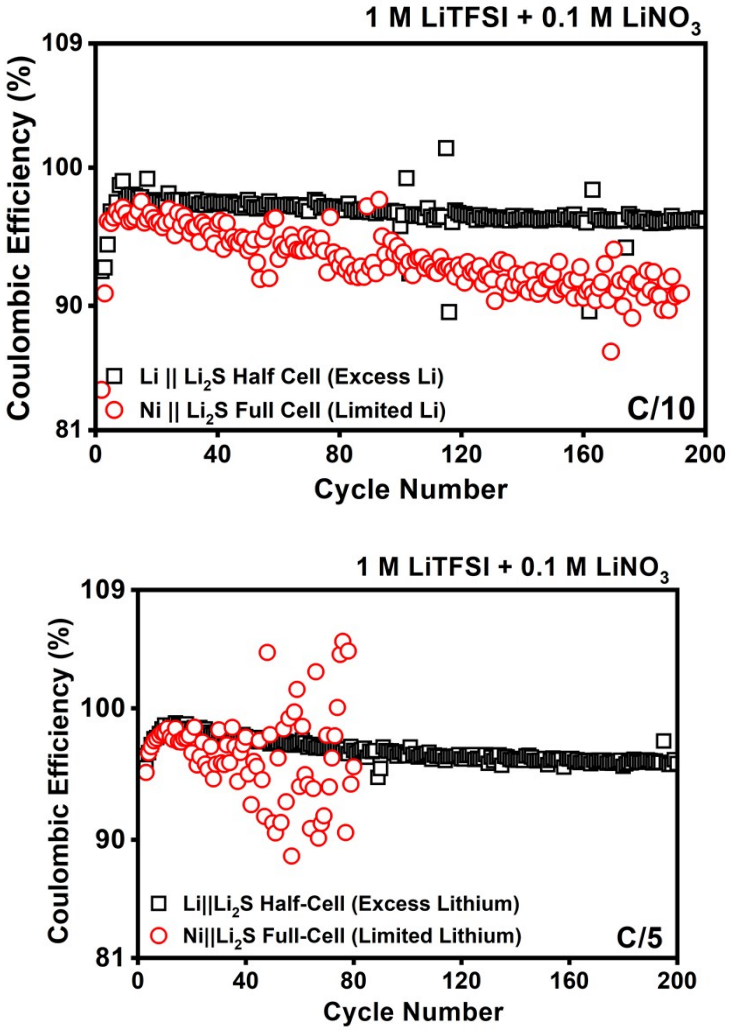

Fig. S3. Coulombic efficiency values for Li || Li_2S half cells and anode-free Ni || Li_2S full cells cycled at C/10 (0.5 mA cm^{-2}) and C/5 (1 mA cm^{-2}) current rates. While the half cells show stable CE values with a general downward trend but with little cycle-to-cycle variation, the anode-free full cells show both a steeper decline in CE values and significantly higher cycle-to-cycle variation. In the advanced stages of cycling, the CE values for the anode-free full cells show erratic fluctuations, indicating cell failure. It should be noted here that the values of Coulombic efficiency significantly overstate the actual lithium inventory loss per cycle as calculated in Fig. 1. The geometric mean of the measured CE values at C/10 rate is 94.9% over 100 cycles, while that at C/5 rate is 96.7% over 40 cycles. If Coulombic efficiency was a perfect predictor of capacity fade, this would imply a lithium inventory loss rate per cycle of 5.1% at C/10 rate and 3.3% at C/5 rate. However, the actual values of lithium inventory loss rates per cycle are 0.6% at C/10 rate and 1.8% at C/5 rate. The discrepancy between the measured values of Coulombic efficiency and actual values of lithium inventory loss rate is due to the internal redox shuttle that is intrinsic to Li-S batteries because of polysulfide intermediates.

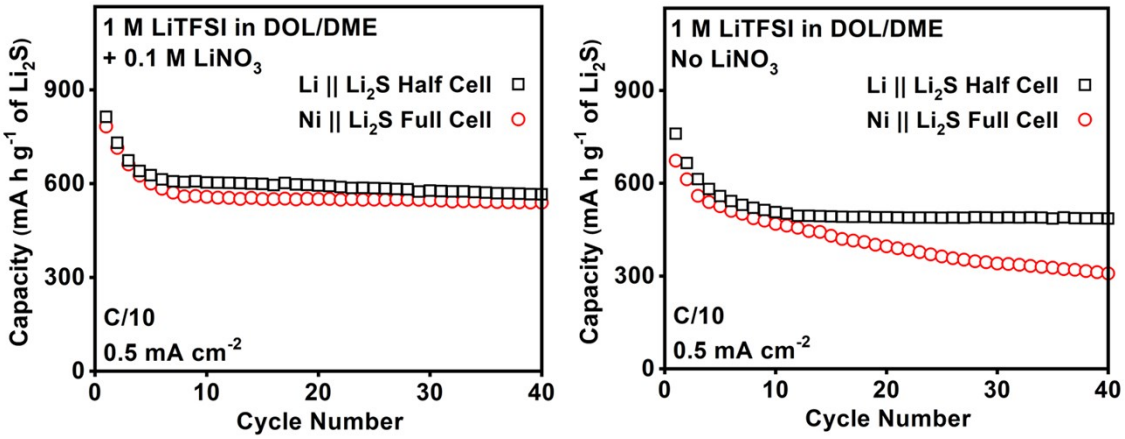

Fig. S4. Electrochemical performance of Li || Li_2S half cells and anode-free Ni || Li_2S full cells cycled with $LiNO_3$-free electrolytes at C/10 rate (0.5 mA cm^{-2}). In the half cell configuration, the $LiNO_3$-free electrolyte shows stable cycling for over 40 cycles. In the full cell configuration, however, the $LiNO_3$-free electrolyte shows a steady decline in capacities, which diverge from the half cell capacities after ~ 10 cycles. This relative trend is in sharp contrast to that observed for the electrolyte with $LiNO_3$.

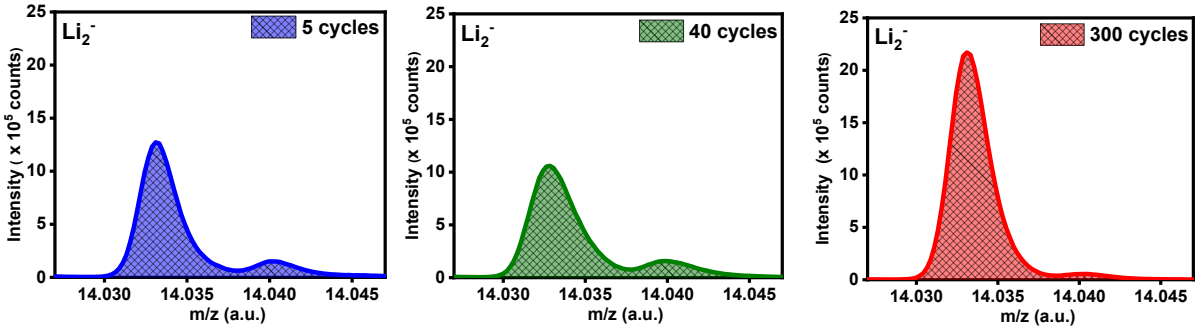

Fig. S5. Integrated intensity for Li_2^- secondary ions in the anode-free Ni || Li_2S full cell after 5, 40, and 300 cycles. Unlike the data shown in Fig. 2a, the intensities in this figure are not scaled with respect to the total ion count registered throughout the sample depth. While the peak area for Li_2^- is significantly higher at 300 cycles compared to 5 and 40 cycles, it should be noted that the total ion count is also roughly two times higher at 300 cycles compared to 5 and 40 cycles. Nevertheless, this figure proves that the main conclusion drawn in Fig. 2, i.e., significant amount of metallic lithium is present even at advanced stages of cycling after cell failure is not an artifact of the normalization process.

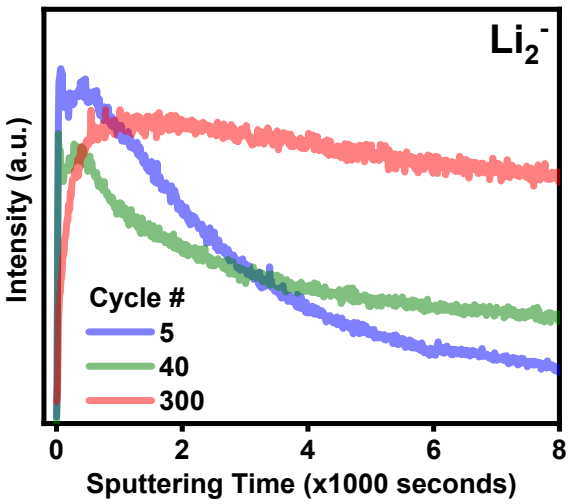

Fig. S6. Depth profiles for Li_2^- secondary ions as a function of sputtering time in the anode-free Ni || Li_2S full cell after 5, 40, and 300 cycles. Unlike the data shown in Fig. 2d, the measured signal is not normalized with respect to the total signal for all secondary ions. Even without the normalization, a significant amount of metallic lithium is observed at 300 cycles. Like the figure above, this shows that the main conclusion drawn in Fig. 2 is not an artifact of the normalization process.

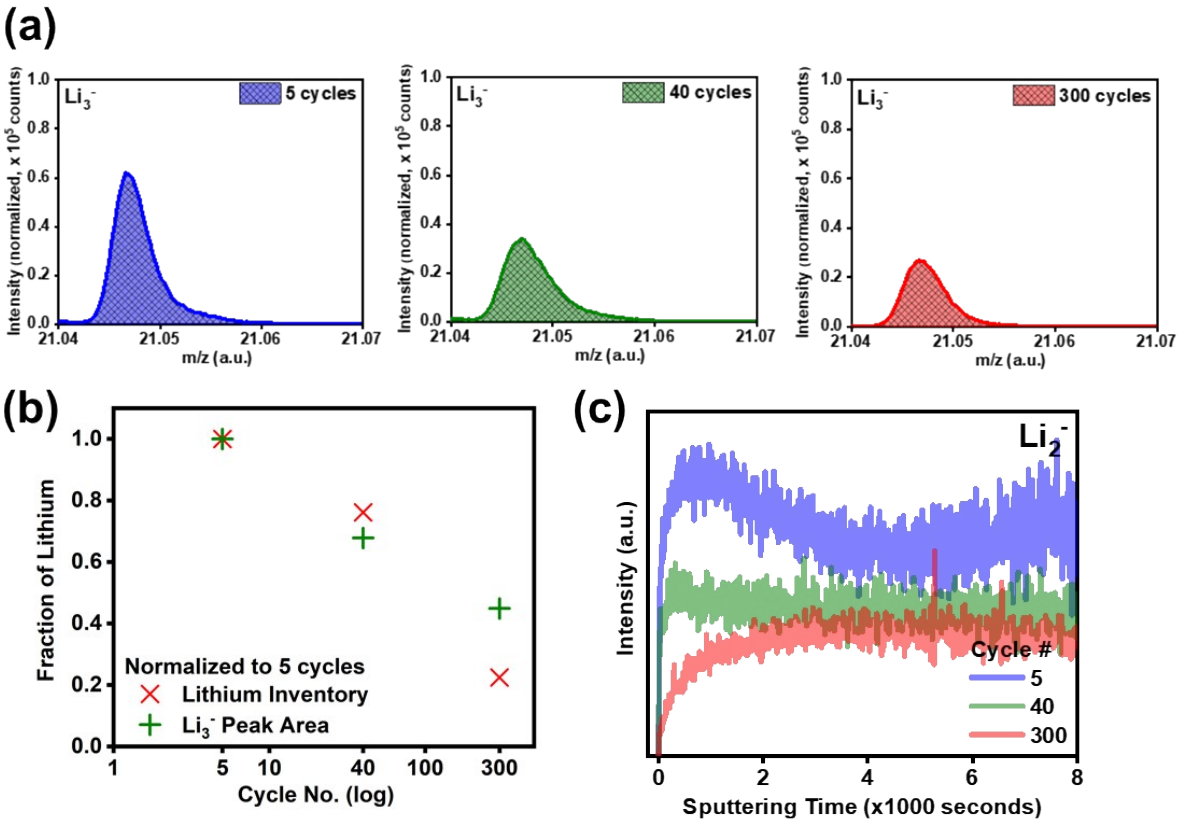

Fig. S7. (a) Integrated intensity for Li_3^- secondary ions in the anode-free Ni || Li_2S full cell after 5, 40, and 300 cycles. Similar to Li_2^-, Li_3^- is also an indicator for metallic lithium. The intensities are scaled with respect to the total ion count registered throughout the sample depth. A progressive reduction in peak area is observed with cycling, although a significant integrated intensity for Li_3^- is still detected at 300 cycles. (b) Lithium inventory retained and total peak area for Li_3^- at 40 and 300 cycles as a fraction of that at 5 cycles. At 300 cycles, a significantly higher peak area for Li_3^- is detected compared to the lithium inventory retained. This indicates the presence of a considerable amount of "dead" metallic lithium. (c) Depth profiles for Li_3^- secondary ions as a function of sputtering time at 5, 40, and 300 cycles. The signals are normalized with respect to the total signal for all secondary ions. Since the signal for Li_3^- is very noisy, Li_2^- secondary ions are chosen in this work as a proxy for metallic lithium. Nevertheless, the relative trend for integrated peak intensities and depth profiles of Li_3^- at 5, 40, and 300 cycles are similar to that for Li_2^-.

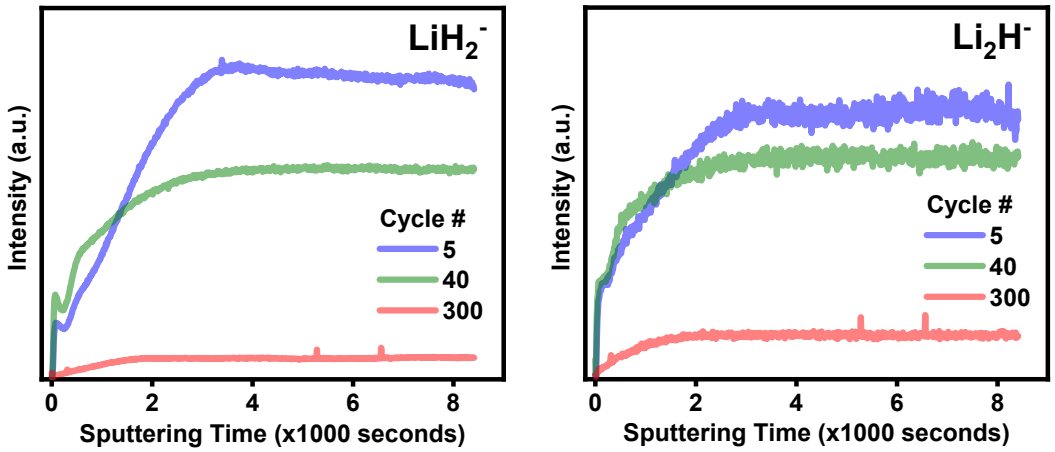

Fig. S8. Depth profiles for LiH_2^- and Li_2H^- secondary ions as a function of sputtering time at 5, 40, and 300 cycles. The signals are normalized with respect to the total signal for all secondary ions. Similar depth profiles are observed as those for H^- and LiH^- secondary ions, which indicates that a sharp boundary between lithium metal and LiH may not be present. Species with intermediate composition between Li and LiH are likely present in the interface. Nevertheless, a reduction in signal intensity is observed with cycling, which is ascribed to possible gas evolution during cell operation.

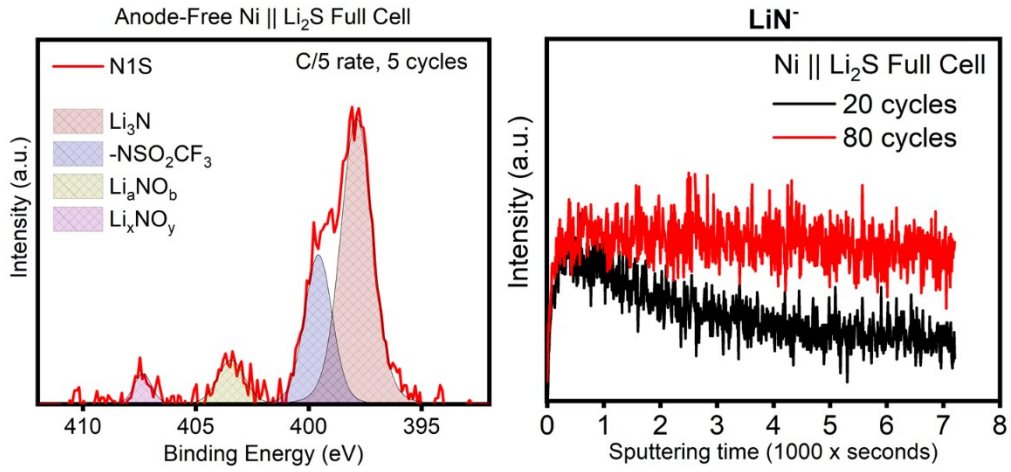

Fig. S9. N1s spectra for the deposited lithium in anode-free Ni || Li_2S full cell cycled at C/5 rate for 5 cycles. Four peaks can be observed corresponding to nitrogen-containing interphasial components. In order of signal intensity, they are Li_3N (~ 397.5 eV), $-NSO_2CF_3$ (~399.8 eV), and two oxidized nitrogen species at ~ 403.8 and ~ 407.5 eV. ToF-SIMS depth profile for LiN^- secondary ion (corresponding to Li_3N) is also shown at 20 cycles and 80 cycles (at C/5), indicating a relatively uniform distribution throughout the deposited lithium and an increase in Li_3N concentration with cycling.

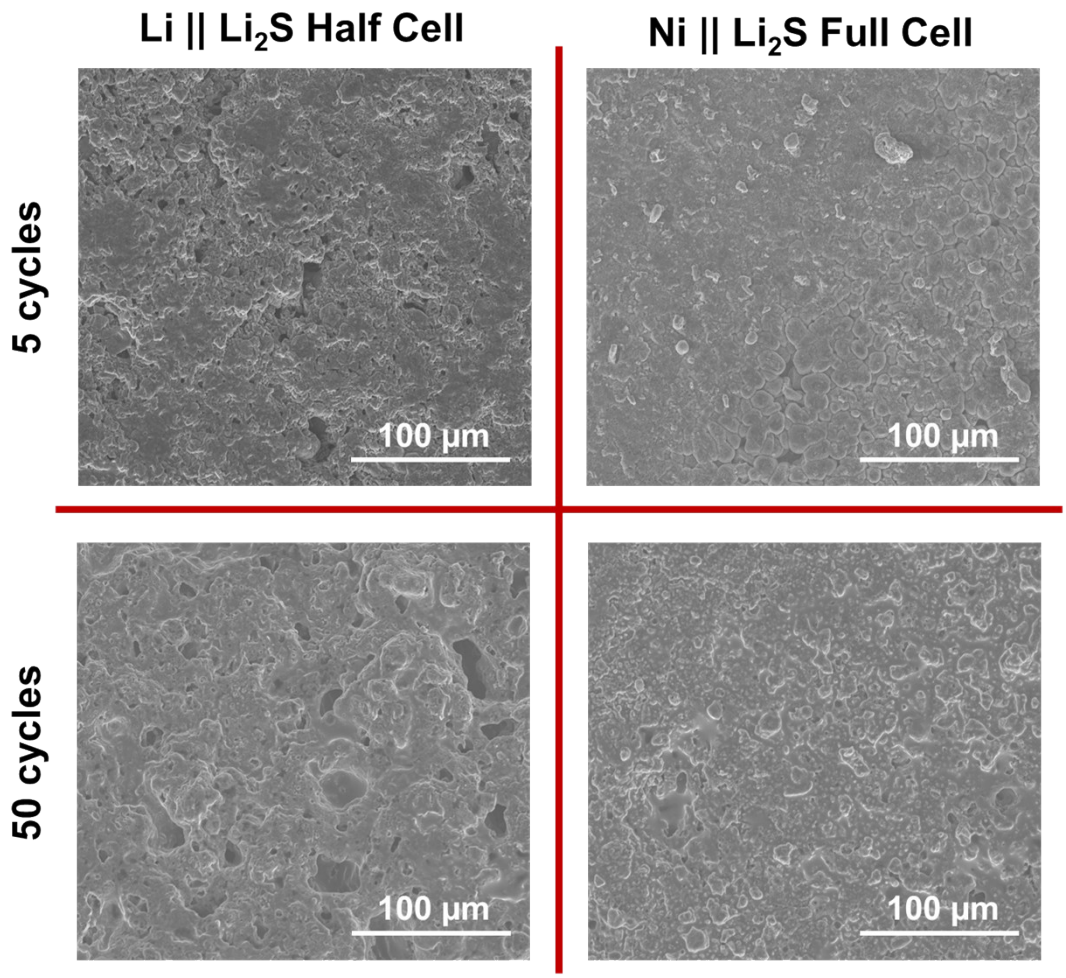

Fig. S10. SEM images of deposited lithium in Li || Li_2S half cells and anode-free Ni || Li_2S full cells cycled at C/5 rate after 5 and 50 cycles. Significant differences in morphology between the half cell and the full cell cannot be discerned. Both systems show relatively smooth and homogenous deposition of lithium at 5 cycles. By 50 cycles, however, the morphology of the plated lithium has deteriorated, and a significantly more non-uniform lithium surface can be observed.

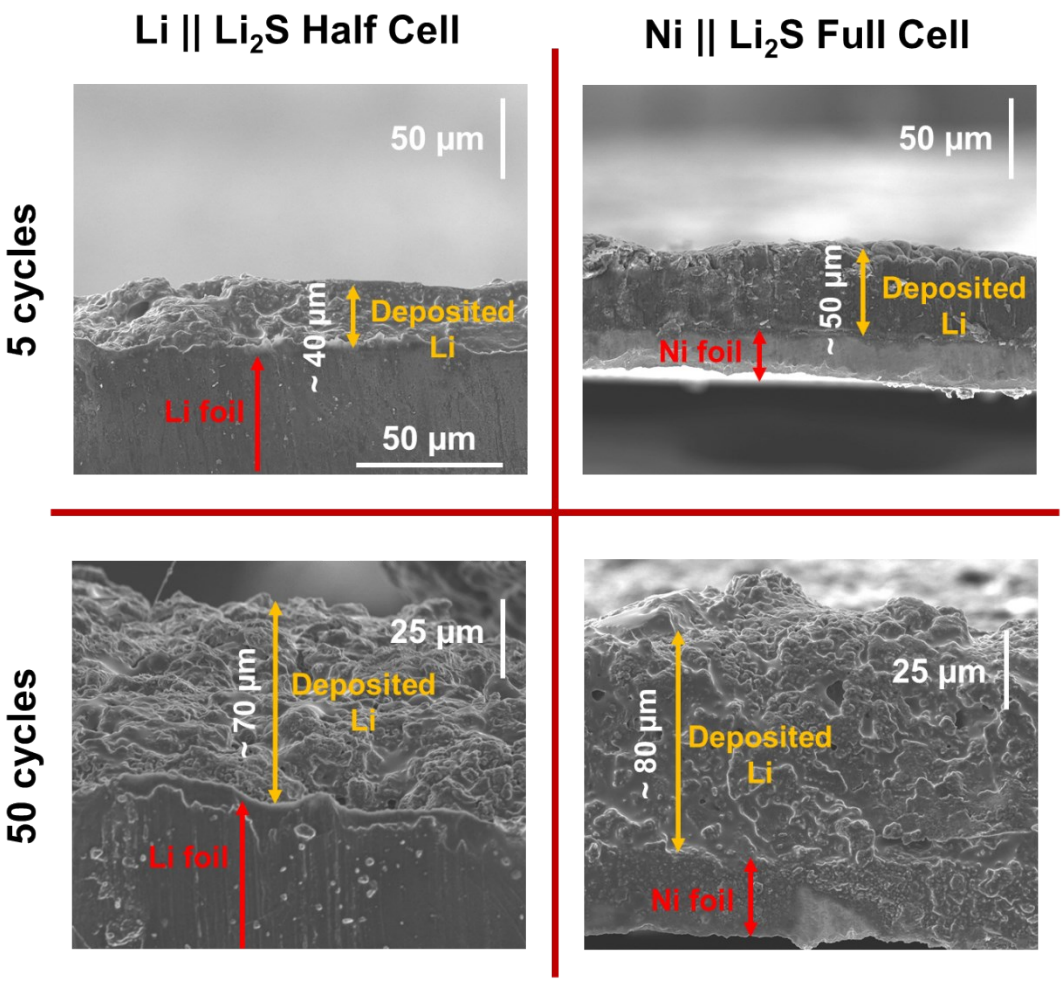

Fig. S11. Cross-sectional SEM images of deposited lithium in Li || Li_2S half cells and anode-free Ni || Li_2S full cells cycled at C/5 rate after 5 and 50 cycles. After 5 cycles, the deposited lithium shows a slightly smaller thickness (40 µm) in the half cell compared to the full cell (50 µm). By 50 cycles, the thickness of the lithium has grown considerably: 80 µm in the full cell and 70 µm in the half cell. Nonetheless, significant differences in the morphology of the deposited lithium still cannot be discerned, with both cases showing relatively uniform and dense plating of lithium initially and the porosity of the lithium deposit increasing considerably with cycling.